Journal of Fluids and Structures 17 (2003) 163–183

JOURNAL OF FLUIDS AND STRUCTURES

www.elsevier.nl/locate/jnlabr/yjfls

Forces on oscillating foils for propulsion and maneuvering

D.A. Read[1], F.S. Hover*, M.S. Triantafyllou

Department of Ocean Engineering, Massachusetts Institute of Technology, Building 5-228, 77 Massachusetts Avenue Cambridge, MA 02139-4307, USA

Received 30 April 2001; accepted 5 July 2002

Abstract

Experiments were performed on an oscillating foil to assess its performance in producing large forces for propulsion and effective maneuvering. First, experiments on a harmonically heaving and pitching foil were performed to determine its propulsive efficiency under conditions of significant thrust production, as function of the principal parameters: the heave amplitude, Strouhal number, angle of attack, and phase angle between heave and pitch. Planform area thrust coefficients of 2.4 were recorded for 35° maximum angle of attack and efficiencies of up to 71.5% were recorded for 15° maximum angle of attack. A plateau of good efficiency, in the range of 50–60%, is noted. A phase angle of 90–100° between pitch and heave is found to produce the best thrust performance. Also, the introduction of higher harmonics in the heave motion, so as to ensure a sinusoidal variation in the angle of attack produced much higher thrust coefficient at high Strouhal numbers. Second, experiments on a harmonically oscillating foil with a superposed pitch bias, as well as experiments on impulsively moving foils in still water, were conducted to assess the capability of the foil to produce large lateral forces for maneuvering. Mean side force coefficients of up to 5.5, and instantaneous lift coefficients of up to 15 were recorded, demonstrating an outstanding capability for maneuvering force production.

1. Introduction

Fish, cetaceans, birds, and insects are, by engineering standards, astoundingly adept flyers and swimmers. The basic source of locomotion and maneuvering forces is the oscillating foil, which can generally undergo simultaneous translation and rotation in two or more degrees of freedom. The foils generate a large-scale vortex wake, which may appear in two distinct forms, one associated with drag and the other with thrust. The drag wake is analogous to the von Kármán street behind a bluff body, wherein the shed vortices induce a velocity in the opposite direction of the mean flow, resulting in a velocity deficit. Under proper conditions, a propulsive oscillating foil reverses the rotational direction in the wake structure so that the vortices induce a velocity in the same direction as the mean flow, creating a velocity excess, that is, a jet. In addition to efficient generation of propulsive force (Hoppe, 1989; Triantafyllou et al., 1993; Anderson et al., 1998) unsteady vortex control creates very high lift coefficients for maneuvering (Gursul and Ho, 1992). An oscillating foil can further be used to manipulate incoming vorticity, and recapture vortical energy (Koochesfahani and Dimotakis, 1988; Cortelezzi et al., 1997; Streitlien et al., 1996; Gopalkrishnan et al., 1994).

Some results on the subject of oscillating foil propulsion focus primarily on flow visualization, while others provide both qualitative and quantitative data on thrust producing foils; we review the contributions of each approach below. The parameters discussed in the papers include reduced frequency $k = \omega c/2U$, Strouhal number $\mathrm{St} = 2\pi A/U$, Reynolds number $\mathrm{Re} = Uc/\nu$, heave amplitude to chord ratio h_0/c, pitch angle amplitude θ, and maximum angle of

*Corresponding author.
E-mail address: hover@mit.edu (F.S. Hover).
[1] Currently with Bath Iron Works Corp., Bath, ME, USA.

0889-9746/03/$ - see front matter
PII: S0889-9746(02)00115-9

Nomenclature

c	foil chord
s	foil span
U	steady towing speed
ρ	fluid density
ν	fluid kinematic viscosity
Re	chord Reynolds number, Uc/ν
$\alpha_{\max}$	maximum of angle of attack $\alpha(t)$
θ_0	amplitude of sinusoidal pitch motion $\theta(t)$
h_0	amplitude of nominally sinusoidal heave motion $h(t)$
ψ	phase angle by which pitch $\theta(t)$ leads heave $h(t)$
V	total velocity vector, induced by $\dot{h}(t)$ and U
A	wake width, approximated as $2h_0$
k	reduced frequency, $\omega c/2U$
St	Strouhal number, $2\pi\omega A/U$
$F_x(t)$	thrust force; mean value $\bar{F}_x$
$F_y(t)$	lift force; mean value $\bar{F}_y$
$P(t)$	mechanical power supplied by actuators; mean value $\bar{P}$
C_T	mean thrust coefficient, $2\bar{F}_x/\rho U^2 cs$
C_L	mean lift coefficient, $2\bar{F}_y/\rho U^2 cs$
$C_{T_{SA}}$	mean thrust coefficient based on approximate swept area, $\bar{F}_x/\rho U^2 h_0 s$
C_L(max)	maximum instantaneous lift coefficient
C_P	power coefficient, $2\bar{P}/\rho U^3 cs$
η	propulsive efficiency, C_T/C_P

attack $\alpha_{\max}$. Here ω is the frequency in rad/s, c is the chord length, and U is the free-stream velocity. Heave amplitude is denoted h_0. The Strouhal number depends on the length parameter A, ideally taken as the width of the wake; A can be estimated using the peak-to-peak excursion of the trailing edge, or more simply by twice the heave amplitude. In this case, the Strouhal number is related to reduced frequency as $\mathrm{St} = 2kh_0/\pi c$. Dynamic properties both at the foil and in the wake are important for a complete characterization (Luznik and Bose, 1998; see also Ohmi et al., 1990, 1991).

Extensive work on flow visualizations pertaining to foils may be found in Scherer (1968), Oshima and Oshima (1980), Oshima and Natsume (1980), Freymuth (1988), Koochesfahani (1989), and Anderson et al. (1998). Freymuth (1988) performed experiments on a NACA 0015 foil in both pure pitch and pure heave. His paper illustrates two examples. For a heaving foil with $k = 2.7$, $\mathrm{Re} = 5200$, $h_0/c = 0.20$, and $\alpha_{\max} = 5^\circ$, a thrust-type vortex street is formed by a weak leading edge separation, which travels down the foil and constructively merges with the trailing edge vortex. For a foil pitching about the quarter-chord point with $k = 2.9$, $\mathrm{Re} = 12\,000$, $\alpha_{\max} = 5^\circ$, and $\theta_0 = 20^\circ$, a similar observation can be made. Larger angles of attack due to pitch or heave result in strong leading edge separation, which weakens the thrust producing qualities of the vortex wake. Furthermore, reducing the frequency of oscillation causes the vortex roll-up of the wake to become more and more sluggish until the usual von Kármán street and associated drag profile again become evident.

Koochesfahani and Dimotakis (1988) conducted more extensive tests on a NACA 0012 foil pitching about its quarter-chord point. At a very small pitch angle (2°), slowly increasing the frequency of oscillation causes the von Kármán street to be modified so that all vortices are first on a line behind the cylinder, and then ultimately are repositioned to create a jet wake, which becomes stronger as the frequency increases. At a larger pitch angle of 4°, the in-line vortex condition does not occur, but is replaced with four vortices per cycle, possibly due to leading-edge vortices. The frequency for vortex roll-up, and therefore the transition to thrust, decreases as the oscillation amplitude increases. In terms of the Strouhal number, however, this transition occurs consistently in neighborhood of $\mathrm{St} = 0.10$.

Anderson (1996) performed digital particle image velocimetry (DPIV) on a foil oscillating in both pitch and heave, and created a vortex pattern map showing wake patterns on a plot of St vs. $\alpha_{\max}$ for large heave amplitudes, up to $h_0/c = 1.0$, and large $\alpha_{\max}$ values. At least six distinct vortex formation regimes exist for the range of parameters, but a region of optimal wake formation, characterized by two vortices per cycle in a reverse von Kármán pattern, occupies

$St = 0.20 - 0.50$ and $\alpha_{max} = 7 - 50^\circ$. The heave ratio h_0/c scales with the strength of the leading edge vortex relative to the trailing edge vortex, so that for the heave ratio $h_0/c = 0.50$, roughly equal-strength vortices are shed from the leading and trailing edges; they coalesce to indicate an optimal thrust-generation condition. Additional experiments were reported by Anderson et al. (1998) for a NACA 0012 foil in pitch and heave, with measurement of thrust and heave force, along with pitching torque. Three heave amplitudes were tested, $h_0/c = [0.25, 0.50, 0.75]$, and the angles covered $\alpha_{max} = [5, 10, 15, 20, 25, 30]^\circ$. St ranged from about 0.05–0.55, with phase angles of $\psi = [75, 90, 105]^\circ$. High efficiency and thrust are generated by the foil under the proper conditions. Specifically, for $h_0/c = 0.75$, $\alpha_{max} = 20.2^\circ$, and $\psi = 75^\circ$, a maximum propulsive efficiency of 87% is obtained at $St = 0.30$. For the same parameters at $St = 0.46$, an efficiency of just over 80% can be obtained with a thrust coefficient of approximately 0.83. The highest thrust coefficient reported is about 1.6 for $h_0/c = 0.75$, $\psi = 90^\circ$, $St = 0.48$, and $\alpha_{max} = 30^\circ$. The efficiency for this same run is just over 70%.

Gursul and Ho (1992) performed novel experiments on stationary airfoils in a flow of oscillating velocity. The foil was set at a given angle of attack and the incoming flow varied according to: $U(t)/U_\infty = 1 + R\cos(\omega t)$, where U_∞ is the average velocity, and R is a dimensionless velocity variation. The mean lift coefficient, defined as $\bar{C}_L = 2\overline{L(t)}\rho U_\infty^2 Lc$, where L is the length of the foil, takes values as high as 2.7, for $\theta = 20^\circ$, $R = 0.70$. The value of k corresponding to this condition is about $k = 0.80$. Additionally, the instantaneous lift coefficient, based on instantaneous lift force and velocity, can be as high as 14. Steady lift coefficients of about one are typical for a airfoil in steady conditions, so these experiments suggest some dramatic effects of the unsteady flow.

One of the principle mechanisms for the high performance in unsteady flow over foils is dynamic-stall (or leading-edge vortices), which occurs when flow separates at the leading edge (Reynolds and Carr, 1985; McCroskey 1982). Dynamic stall has been discussed in insect flight by Maxworthy (1979), Ellington (1984), Freymuth (1990), Rayner (1995), and Liu et al. (1998). In particular, Ellington (1984) and Ellington et al. (1996) noted that stall is delayed during oscillatory loading, as seen by Maresca et al. (1979). An additional point on biological wings pertains to three-dimensional effects; lift-induced drag is reduced due to the alternating sign of the tip vortices (Cheng and Murillo, 1984) and lead to the "concertina" wake behind flying birds (Lighthill, 1969; Rayner, 1979). The three dimensionality of flapping wings and fins has also been studied by Hart et al. (1992) Dickinson et al. (1999), and Drucker and Lauder (1999).

The present paper details a series of propulsion and maneuvering experiments performed with a heaving and pitching foil section, with measurement of lift and thrust forces, and pitching torque. First, we show systematic maps of efficiency and thrust coefficient, which indicate specific conditions of high performance under significant thrust production. Next, we performed tests on a flapping foil with a bias angle to measure the instantaneous and mean lift coefficient, which can generate the forces needed for maneuvering. Finally, we consider one-time impulsive maneuvers in still water, which are capable of generating extremely large instantaneous forces. With respect to applications, recent work on underwater vehicle propulsion and maneuvering has been performed by, e.g., Bandyopadhyay et al. (1997) and Kato (1998).

2. Experimental setup and methods

2.1. Apparatus

All experiments were conducted in the MIT Department of Ocean Engineering Testing Tank. The water tank itself is rectangular, with 18 m working length 2.6 m width, and 1.4 m depth. A mobile carriage, shown in Fig. 1, contains the complete motion control and sensor system. A large servomotor positions the lower carriage through a linear bearing table, and a separate motor pitches the foil through a chain drive. Sensed variables include the vertical position of the foil (LVDT and heave motor encoder), angular position of the foil (potentiometer), pitch torque about the 1/3-chord pivot point, and forces exerted by the foil in the horizontal and vertical directions. We employed Kistler piezoelectric load cells for the torque and force measurements.

The foil used for all the experiments is rectangular with constant NACA 0012 section, chord 10 cm, and span 60 cm. It was constructed primarily of wood, with a fiberglass cloth and resin covering that provided an exceptionally smooth finish. Stainless-steel axles were inserted on each end of the foil at the 1/3-chord position. Endplates were used on each strut to prevent flow around the ends of the foil and maintain approximately two-dimensional flow; the gap between plate and foil on each side was maintained at less than 2 mm.

Regular calibration verified consistently that all the sensors were linear to within 1.5% of the ranges encountered in the experiments. In addition to regular calibration, the pitch zero position was adjusted until the foil produced no lift.

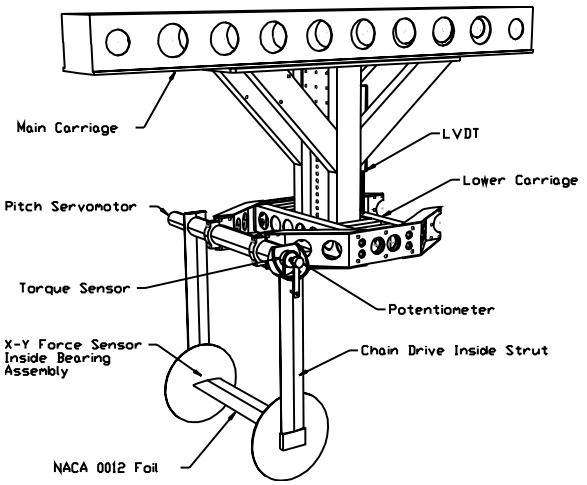

Fig. 1. View of the test carriage, which oscillates the foil in heave and pitch, while moving horizontally in a towing tank.

Finally, we performed tests to ensure that the extrapolation of force measurement at one end only was valid for loads applied across the span. The towing speed, U, was 0.40 m/s for all runs, corresponding to $\mathrm{Re} = 4 \times 10^4$.

One of the most important parameters in this study is the Strouhal number based on heave amplitude:

$$\mathrm{St} = \frac{4\pi h_0 \omega}{U}, \tag{1}$$

where h_0 is the heave amplitude, ω is the circular frequency in rad/s, and U is the velocity. As noted previously, the $2h_0$ term is an estimate of the width of the foil wake A. Although the motion of the trailing edge is likely a better estimate of the wake width, for the purposes of these experiments with $\psi \approx 90^\circ$, they are very close.

The average thrust force in propulsion tests is computed as follows:

$$\bar{F}_x = \frac{1}{T}\int_0^T F_x(t)\,\mathrm{d}t \quad \text{for } T >> 2\pi/\omega, \tag{2}$$

where the thrust force is taken with reference to zero forward speed, and the mechanical power delivered by the motors is given as

$$\bar{P} = \frac{1}{T}\left(\int_0^T F_y(t)\dot{h}(t)\,\mathrm{d}t + \int_0^T Q(t)\dot{\theta}(t)\,\mathrm{d}t\right). \tag{3}$$

Force data are reduced to coefficient form using the following equation:

$$C = \frac{F}{\frac{1}{2}\rho U^2 cs}. \tag{4}$$

In most cases U represents the towing velocity, but for impulsive-start experiments, where the carriage speed is zero, U represents the *maximum* heave velocity. F denotes a measured force; in this work, F can represent either the thrust or lift components; C_T denotes the thrust coefficient and C_L the lift coefficient. The coefficients can also be instantaneous or the average over several cycles. The thrust and power coefficients are therefore

$$C_T = \frac{\bar{F}_x}{\frac{1}{2}\rho cs U^2}, \tag{5}$$

$$C_P = \frac{\bar{P}}{\frac{1}{2}\rho cs U^3}. \tag{6}$$

Propulsive efficiency is then given simply as

$$\eta = \frac{C_T}{C_P}. \tag{7}$$

Thrust and power coefficients may alternatively be defined by the swept area of the trailing edge instead of the planform area of the foil. As with the Strouhal number, this area can be approximated by just the product of span and double heave amplitude. For example, Eq. (6) then becomes

$$C_{T_{SA}} = \frac{\bar{F}_x}{\rho h_0 s U^2}. \tag{8}$$

In the results shown, C_T is defined as in Eq (6); to convert C_T to $C_{T_{SA}}$, one must multiply by $1/2$ if $h_0/c = 1.0$, and by $2/3$ for $h_0/c = 0.75$.

2.2. Foil trajectory

Most of the propulsion experiments were conducted using sinusoidal motion for both the heave and pitch degrees of freedom. The heave and pitch motions are

$$h(t) = h_0 \sin(\omega t), \tag{9}$$

$$\theta(t) = \theta_0 \sin(\omega t + \psi), \tag{10}$$

so that ψ is the phase angle between pitch and heave in radians. The resulting angle of attack profile is related to the heave velocity and pitch angle (see Fig. 2):

$$\alpha(t) = -\arctan\left(\frac{\dot{h}(t)}{U}\right) + \theta(t). \tag{11}$$

The normal procedure is to fix U, ω, h_0 (thus defining the Strouhal number), phase angle ψ, and $\alpha_{\max}$. We then solve for the absolute pitch angle magnitude θ_0. An approximation for $\psi \simeq \pi/2$, and valid for low St, where the function $\arctan(x)$ is nearly linear in x, is

$$\theta_0 = \pi \mathrm{St} + \alpha_{\max}. \tag{12}$$

The phasing of $\alpha_{\max}$ with regard to the harmonic motion in heave and pitch varies greatly over this parametric set. In fact, the above equation has two solutions over a large range of frequencies, one corresponding to drag production, and the other to thrust generation. This double solution in the angle of attack equation results from the fact that the foil can be pitched up or down with respect to the instantaneous oncoming flow. Fig. 3 shows two θ_0 solutions, for the case $\alpha_{\max} = 15^\circ$ and several phase angles. The circled points are the terminal Strouhal numbers; the point where the thrust- and drag-producing values of θ_0 converge for each phase angle.

The angle of attack profile itself takes various forms, depending on the proximity of the θ_0 solution to the bifurcation point, i.e. the terminal Strouhal number. For example, in Fig. 4, the lowest value of St achieves nearly sinusoidal $\alpha(t)$, but as St increases, the α profile degrades sharply, through growing odd harmonics. In the case of $\psi \neq 90^\circ$, the changes in $\alpha(t)$ evolve asymmetrically, but are otherwise similar.

The irregular angle of attack signal induced by high St could be eliminated through modifications to either or both the trajectory of $\theta(t)$ and $h(t)$. Without careful testing it would be difficult to assess clearly what combination of effects is best for recovering thrust. In this work, we consider a correction using heave alone. In short, we expand $\dot{h} = U \tan(\theta(t) - \alpha(t))$ using a power series, with the assumption of harmonic $\theta(t)$ and $\alpha(t)$. We then compute n (odd)

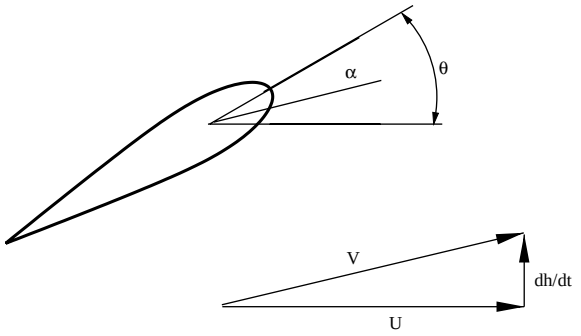

Fig. 2. Foil kinematic parameters, showing the relationship between physical pitch angle, and angle of attack.

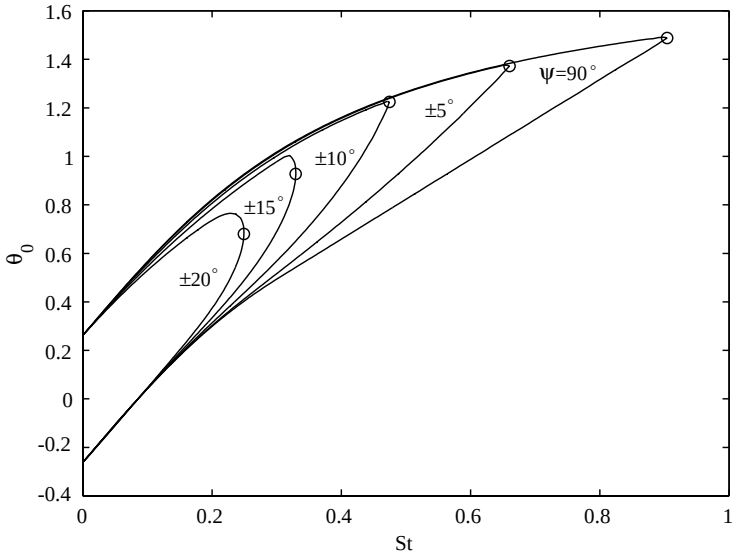

Fig. 3. Bifurcation of the equation for maximum angle of attack α_{max}, showing both thrust- and drag-producing solutions, for $\alpha_{max} = 15^{\circ}$.

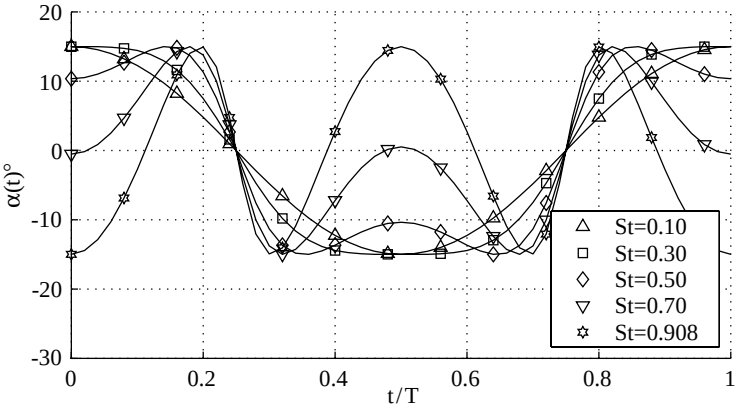

Fig. 4. Angle of attack profile showing the result of increasing Strouhal number for $\psi = 90^{\circ}$, $\alpha_{max} = 15^{\circ}$. The large variations in $\alpha(t)$ are induced by the arctangent function, and cause degraded performance.

super-harmonic components in $\dot{h}$, which cancel out terms induced by the tangent function. This procedure can be streamlined so that one needs only to solve a well-posed n-dimensional linear system. The result is coefficients to be implemented as: $\dot{h}(t)/U = H_1 \sin(\omega t) + H_3 \sin(3\omega t) + H_5 \sin(5\omega t) + \cdots$). The effect of the third and fifth harmonics via this approach is shown in Fig. 5; note that the graph shows $h(t)$ nondimensionalized with U and ω. The third and fifth harmonics change the baseline heave motion by less than 6% for the St range in this work, and so can be implemented easily.

3. Propulsion experiments

3.1. Results for simple harmonic motion

In Figs 6 and 7 we show the overall results of experiments conducted at $h_0/c = 0.75$ and 90° phase angle. Oscillations up to about 1.2 Hz were possible, giving a maximum Strouhal number of 0.44; α_{max} covers the range $[10–40]^{\circ}$. Contours are calculated from experimental points taken at increments of 0.04 in St and 5° in α_{max}. At least two runs were conducted at each point to validate repeatability.

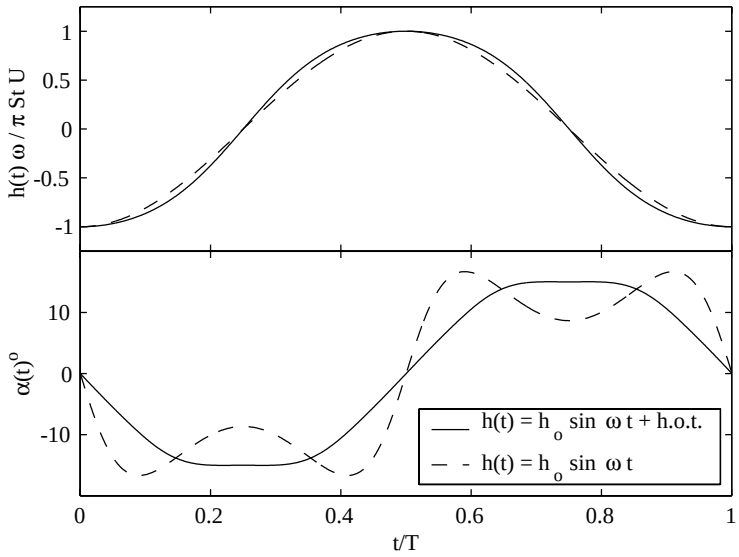

Fig. 5. Effect of higher-order heave motion on angle of attack profile for $\psi = 90°, \mathrm{St} = 0.60, \alpha_{\max} = 15°$. A reasonable perturbation in the heave motion corrects the degraded $\alpha(t)$ profile.

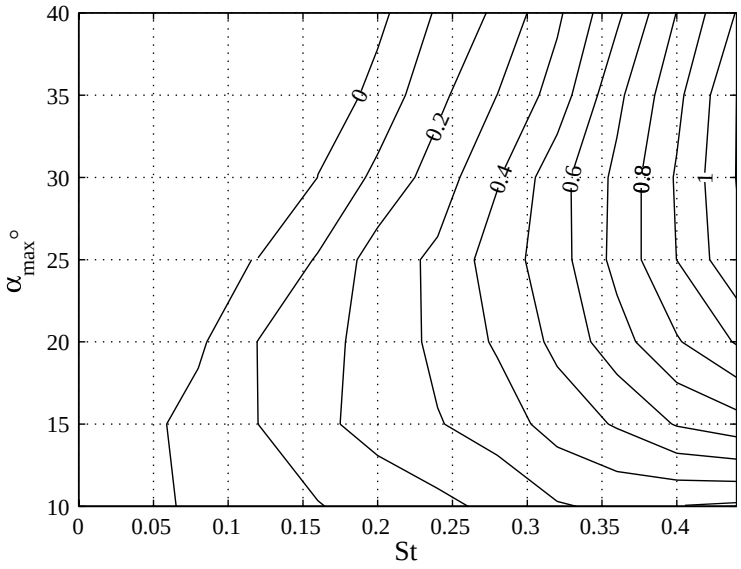

Fig. 6. Contours of thrust coefficient for $h_0/c = 0.75$ and $\psi = 90°$.

C_T increases uniformly with St for high $\alpha_{\max}$, but at lower values of $\alpha_{\max}$, the available C_T levels off. At $\alpha_{\max} = 10°$, for instance, the highest value is $C_T \approx 0.3$, achieved at the relatively low value $\mathrm{St} = 0.32$. A maximum thrust coefficient of 1.10 exists around 30° $\alpha_{\max}$ and $\mathrm{St} = 0.44$ (the upper limit). At the other extreme, the zero contour of C_T represents the transition in the wake between drag- and thrust-producing vortex patterns. At low maximum angles of attack, this zero-crossing occurs at a low Strouhal number, around 0.06. As $\alpha_{\max}$ increases, the transition occurs at higher and higher St.

A maximum propulsive efficiency of 71.5% was achieved at $\alpha_{\max} = 15°$ and $\mathrm{St} = 0.16$ (Table 1). This high efficiency peak is concurrent with a low thrust coefficient of only 0.18, however. Much more significant is the large 50%+ level of efficiency in the region of $\mathrm{St} > 0.15$ and $\alpha_{\max} = 15-25°$. In this regime, we find a run with 55.6% efficiency and $C_T = 0.79$, at $\alpha_{\max} = 20°$ and $\mathrm{St} = 0.40$. Similarly, at $\alpha_{\max} = 25°$ and $\mathrm{St} = 0.44$, we observe 50.8% efficiency and $C_T = 1.08$. These thrust coefficients correspond to swept-area thrust coefficients of $C_{T_{SA}} = 0.53$ and 0.72, respectively.

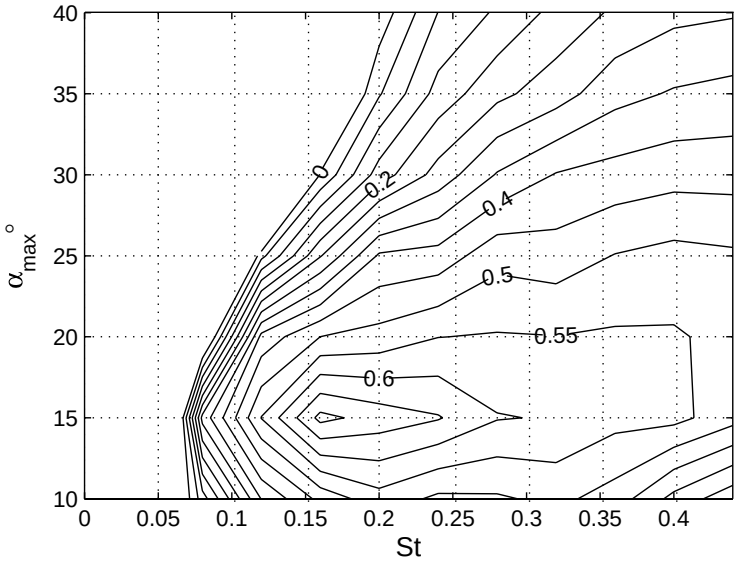

Fig. 7. Contours of efficiency for $h_0/c = 0.75$ and $\psi = 90^\circ$.

Table 1
Higher-harmonic components used for $\alpha_{max} = 15^\circ$, as a function of Strouhal number, and for $\psi = 90^\circ$

St	H_1/πSt	$H_3/3\pi$St	$H_5/5\pi$St
0.20	1.010	-0.010	0.000
0.24	1.014	-0.015	0.000
0.28	1.019	-0.019	0.001
0.32	1.023	-0.024	0.001
0.36	1.028	-0.029	0.001
0.40	1.032	-0.034	0.002
0.44	1.036	-0.038	0.002
0.48	1.040	-0.043	0.002
0.52	1.044	-0.047	0.003
0.56	1.048	-0.051	0.003
0.60	1.051	-0.055	0.004

Figs 8 and 9 show the results of experiments conducted with a somewhat higher heave amplitude: $h_0/c = 1.00$, with $\psi = 90^\circ$. Oscillations up to about 1.2 Hz were again possible, with the higher heave amplitude giving a maximum Strouhal number of 0.60. Maximum angle of attack varies from 10° to 50° for these tests.

The maximum thrust coefficient achieved is significantly higher than with $h_0/c = 0.75$, largely because of the larger Strouhal numbers which can be reached at the same dimensional frequency. For example, the highest C_T-value is 2.20 at $\alpha_{max} = 35^\circ$ and St = 0.60. At the value St = 0.44, the limit of the $h_0/c = 0.75$ tests, we see $C_T \approx 1.15$ as a maximum value, achieved with $\alpha_{max} = 25-30^\circ$; these results are close to those obtained with $h_0/c = 0.75$. Higher thrust is the product of larger motions, but efficiencies are slightly reduced, as might be expected from ideal propeller considerations. For instance, the highest C_T achieved with $h_0/c = 1.0$ corresponds with $\eta = 0.37$.

The peak efficiency of 63.4% (St = 0.20, $\alpha_{max} = 15^\circ$), as before, correlates with a fairly low thrust coefficient of only 0.22. The efficiency contours show, however, that the $\eta = 50\%$ level extends all the way from St = 0.15 ($\alpha_{max} = 15-20^\circ$), to St = 0.60 ($\alpha_{max} = 17-27^\circ$). The high-St portion of this plateau corresponds with high thrust and efficiency: At $\alpha_{max} = 25^\circ$ and St = 0.60, we find an efficiency of 55.6% and $C_T = 2.05$. This number translates to a swept area thrust coefficient of about $C_{T_{SA}} = 1.03$. These numbers reflect useful application to propulsion.

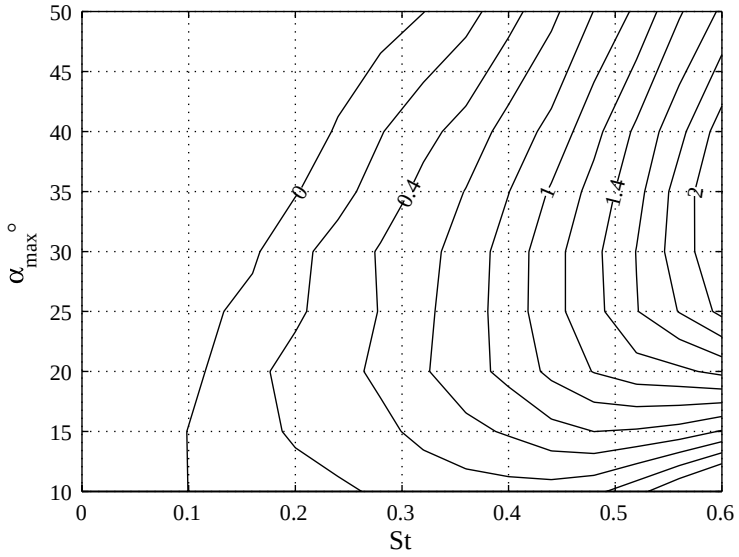

Fig. 8. Contours of thrust coefficient for $h_0/c = 1.00$ and $\psi = 90^\circ$.

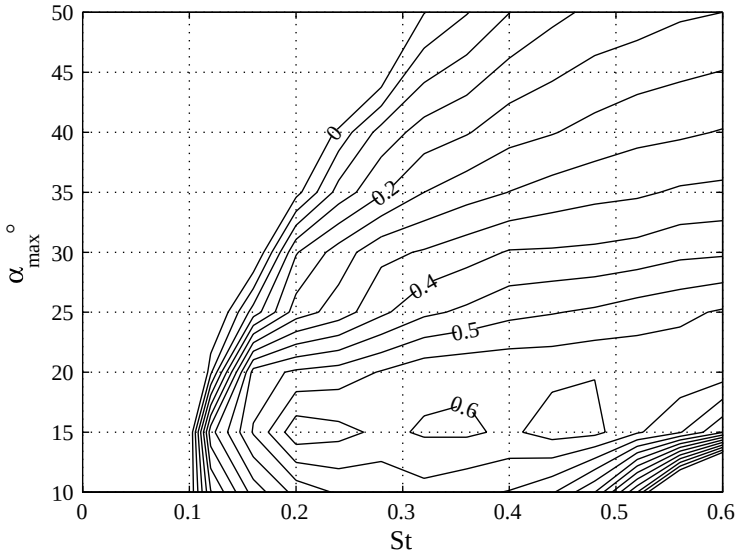

Fig. 9. Contours of efficiency for $h_0/c = 1.00$ and $\psi = 90^\circ$.

Again we note the zero-level contour of thrust coefficient. Trends are similar to those for the case $h_0/c = 0.75$, with the zero crossing at lower Strouhal number for low α_{max} ($10-15^\circ$) and increasing for high angles of attack. With $h_0/c = 1.00$, however, the transition starts at $St = 0.10$ for low angles of attack and increases to about $St = 0.23$ for 40° angle of attack. At the highest angle of attack of 50°, which we did not test for $h_0/c = 0.75$, the transition occurs at a Strouhal number of over 0.32. Hence, drag can occur at values of St well within a high-efficiency operating range, if the angle of attack is too large.

Also of interest at $h_0/c = 1.0$ is the transition from thrust *back* to drag for high St and low α_{max}. We see this in Fig. 8 for 10° angle of attack and $St \geq 0.54$. As discussed previously, lower angles of attack at high Strouhal number are more susceptible to multi-peaked angle of attack profiles. In this case, the angle of attack profile has become distorted enough to cause the foil to produce drag.

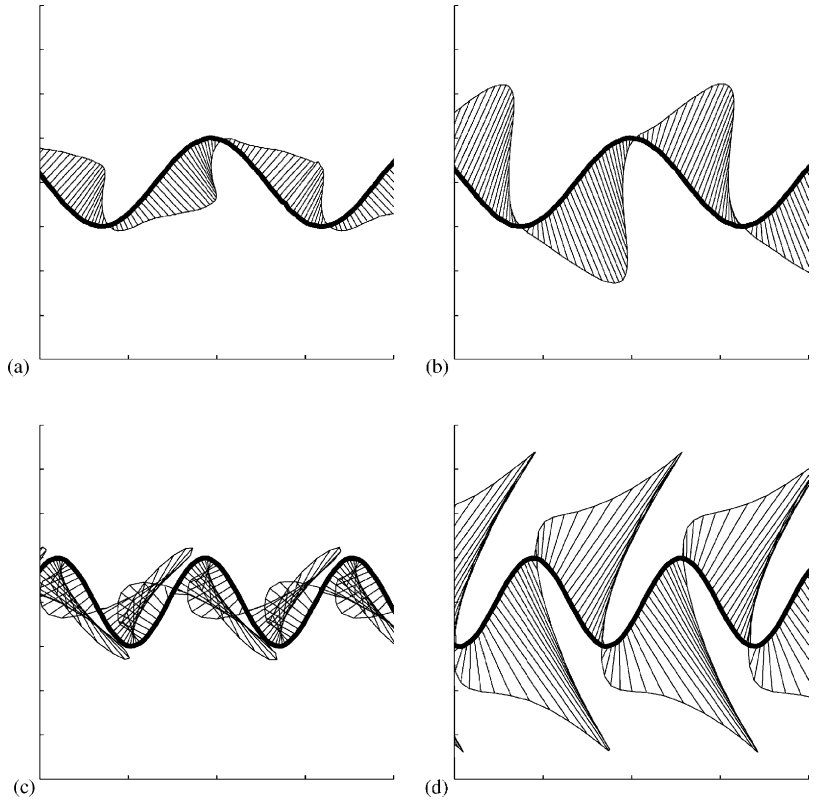

Fig. 10. Thrust vectors for $\psi = 90^\circ$, showing the large magnitude of transient lift forces: (a) $\alpha_{max} = 15^\circ$, St = 0.40; (b) $\alpha_{max} = 35^\circ$, St = 0.40; (c) $\alpha_{max} = 15^\circ$, St = 0.60; (d) $\alpha_{max} = 35^\circ$, St = 0.60. The foil is moving left to right, and the aspect ratio of the force lines shown is 1:1.

In general, some parametric combinations show promise for propulsion. Efficiency is quite high in some cases, but these peaks are not paired with good thrust performance. Large thrust coefficients are attainable with moderate to good efficiency, however. Both heave amplitudes show similar thrust performance, but lower mechanical frequencies allowed us to reach higher Strouhal numbers with the higher heave amplitude. On the other hand, the swept area thrust coefficients $C_{T_{SA}}$ are higher for the lower heave amplitude. Efficiency at low Strouhal number is better for $h_0/c = 0.75$, while efficiency at high Strouhal number (in the range of good thrust performance) appears slightly better for $h_0/c = 1.00$.

To this point, we have described results for time-averaged forces on the foil, namely C_T and η. The actual forces generated are unsteady functions of time, and vary greatly over one period of oscillation. In Fig. 10, we plot instantaneous force magnitude and direction with relation to heave position. We show the results for two values of α_{max}, 15 and 35°, and two Strouhal numbers, 0.40 and 0.60. The foil travels left to right, and all four vector plots have $h_0/c = 1.0$

For St = 0.40, and 15° angle of attack, the instantaneous force vectors result in a relatively high efficiency (60%), and moderate thrust coefficient (0.62). For 35° maximum angle of attack the efficiency was much lower (30%), and the thrust coefficient was higher (0.80). In both of these cases, a large amount of oscillating lift is generated to produce a relatively small amount of mean thrust. In other words, most of the force created by the foil is vertical, with a relatively small horizontal component.

Since these runs were conducted at the same Strouhal number, towing speed, and heave amplitude, they have identical heave velocities as a function of time. Looking at Eq (3) we see that it is the lift component of the power into the system that has to be elevated for the $\alpha_{max} = 35^\circ$ case; the torque component of the power is usually small compared to the lift, say 10% of the total. The proportion of lift to thrust will be discussed further in the next section.

For St = 0.60, the maximum value tested, and $\alpha_{max} = 15^\circ$, the thrust coefficient was 0.58 and the efficiency was 40%. Both thrust and efficiency curves are dropping off at this point, and it is probable that thrust transitions back to drag at a slightly higher Strouhal number. As can be seen from the force vectors in Fig. 10, these parameters exhibit a deformed angle of attack profile. Indeed, the largest forces occur near the point where the heave velocity is zero and the smallest

forces occur where the heave velocity is near its maximum. For the 35° maximum angle of attack case at St = 0.60, thrust is very high, at $C_T = 2.2$; the efficiency was 36%. The magnitude of the total force vectors is now quite large at nearly every point in the heave cycle, with a very brief period of small magnitude at zero heave velocity. The thrust component of the force vectors is again small compared to the lift component, but the magnitude of the forces is so large that a relatively high thrust component is produced anyway.

3.2. Effects of phase angle

The previous section discusses results with the phase angle fixed at $\psi = 90°$, pitch leading heave. We now consider the effects of varying ψ. A set of experiments were conducted with $h_0/c = [0.75, 1.00]$, $\alpha_{max} = 15-35°$, and $\psi = 70-110°$. In general, the same trends with ψ were identified for each condition, and we show in Fig. 11 some typical results. Overall, there is little benefit to phase angles other than 90°, although some interesting properties are evident.

A distinct decrease in thrust coefficient eventually occurs with increasing Strouhal number for any phase angle, but the value $\psi = 90°$ appears to be the most robust. As discussed in Section 3, a given angle of attack is not achievable above a certain Strouhal number for a given phase angle; Fig. 3 shows with circles the terminal Strouhal numbers for all of the phase angles tested. The St$-\theta_0$ pair representing the convergence of drag- and thrust-producing θ_0 values is located at this terminal Strouhal number. In the experiments, then, the $\psi = 90°$ condition emerges as the most robust because the two solutions are distinct for the entire range of St tested. At lower h_0/c, we did not attain a high enough Strouhal number to see this trend, since 90° phase is the least susceptible to distortion. As an aside, we note that the phase angles above 90° generally create higher thrust than do those below, even though the bifurcation calculations indicate a rough symmetry of α distortions.

We observe similar results for $h_0/c = 0.75$ and 1.0, but are able to investigate higher Strouhal numbers in the latter case. A large efficiency gain of around 11% exists for $\psi = 70°$ at St = 0.16. This peak, however, occurs at a low Strouhal number and has a low thrust coefficient. We note also the flat shape of the efficiency curve for 90°, which was noted in Section 3.1.

Fig. 11 shows various, mild increases in efficiency over the entire range of Strouhal numbers tested; peaks occur in different parts of the St range for different phase angles. In the range St = 0.24–0.36, for example, $\psi = 110°$ shows the most benefit, with a maximum improvement of around 8% at Strouhal number 0.28. The highest efficiency for St = 0.40–0.48 occurred at $\psi = 100°$, with a maximum improvement of about 6% at St = 0.44. In the highest range of Strouhal numbers, from 0.48 to 0.60, $\psi = 80°$ shows improvement, with a maximum benefit of about 5% at St = 0.52. The benefits in efficiency for 100° and 110° phase angle are matched by corresponding gains in thrust coefficient.

With $\alpha_{max} = 25°$, the thrust curve for $\psi = 90°$ shows no sign of decline even up to St = 0.60. The case of $\psi = 100°$, also shown, generally provides an enhanced thrust coefficient, but only up to a certain Strouhal number. This benefit was observed to extend to a higher value of St as α_{max} increases, and experiments with $\psi = 100°$, $\alpha_{max} = [30, 35]°$ were

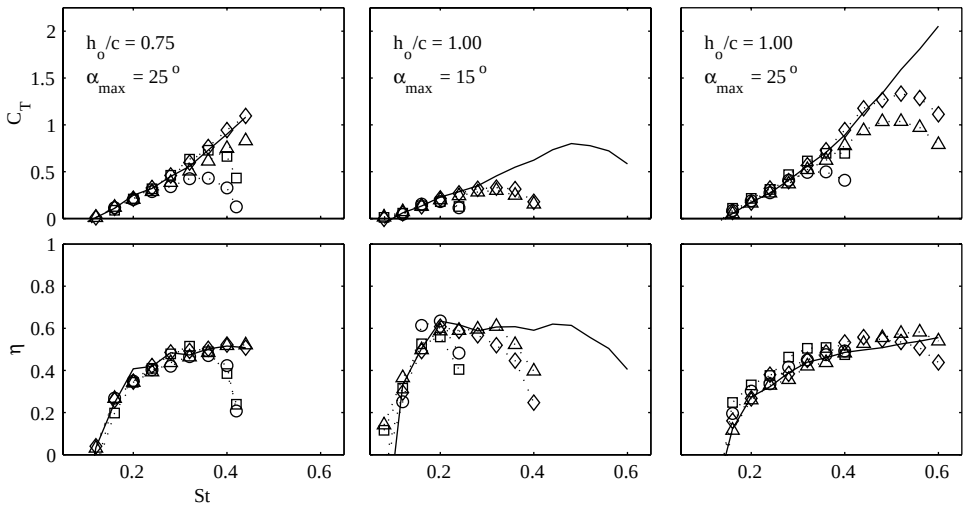

Fig. 11. Effect of phase angle for three typical cases. ◦: $\psi = 70°$, △: $\psi = 80°$, —: $\psi = 90°$, ◇: $\psi = 100°$, □: $\psi = 110°$. Although slight improvements are seen for a few cases, the choice $\psi = 90°$ gives the best performance.

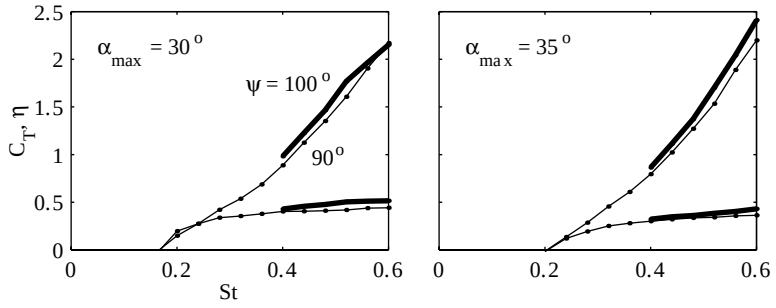

Fig. 12. Effect of 100° phase angle for $h_0/c = 1.00$.

conducted. Fig. 12 shows the results of these experiments, and confirms a general increase in both efficiency and thrust coefficient for $\psi = 100°$, in the range tested. For $\alpha_{max} = 30°$, C_T is consistently higher up to a Strouhal number of 0.52, where the slope of the curve begins to decrease. At Strouhal number 0.60, both values of thrust coefficient are about 2.16. The efficiency at this point is 51.5%, or 6% higher than that for the $\psi = 90°$ test. At Strouhal number of 0.52, the difference in performance is clearer: $C_T = 1.77$ for $\psi = 100°$ while $C_T = 1.60$ for $\psi = 90°$. Efficiency here increases from 41.9 to 50.3%, an 8.4% increase.

For $\alpha_{max} = 35°$, the thrust coefficient with $\psi = 100°$ is higher than that of $\psi = 90°$ all the way up to St = 0.60. Peak performance is attained at the highest Strouhal number, 0.60, with a thrust coefficient of 2.41 and efficiency of 43.1%.

In summary, phase angles other than 90° can improve propulsive performance in certain parametric ranges. At the lower values of α_{max}, occasional efficiency gains of 5–10% are possible, but this is at the cost of thrust performance, which declines markedly at higher Strouhal numbers. Note that as Fig. 3 is remapped for higher α_{max}, the terminal Strouhal number increases for every phase angle.

3.3. Higher-order heave motion

The previous section demonstrated small efficiency increases for phase angles other than the nominal value of 90°. However, if these efficiency increases occur at high St (i.e. close to the terminal value), they are generally accompanied by declining thrust performance associated with distorted angle of attack profiles. More frequently, however, phase angles other than 90° showed worse efficiency at high Strouhal number, mimicking the decline in thrust performance. In an effort to recover this lost performance, foil kinematics were altered in such a way that the angle of attack profile retained a generally sinusoidal shape, avoiding forms with more than two peaks per cycle. Namely, the heave motion was changed to include third and fifth order terms, as described in Section 3. The results of the experiments conducted with this higher-order heave motion are given in Table 2. All experiments of this type were conducted at $h_0/c = 1.00$.

As an example case, Fig. 13 indicates that the effect of the higher-order heave motion is a continuation of the nominal C_T vs. St line, which normally degrades with the angle of attack at high St. Efficiency is also sustained at a plateau by the higher-order motion, whereas with sinusoidal heave motion, it typically falls off to very poor levels at high St.

At $\psi = 90°$ there is significant improvement in efficiency due to the higher-order heave motion for $\alpha_{max} = 15°$, but a smaller effect at $\alpha_{max} = 20°$. This characteristic can be predicted from the contour plots of Section 4.1, in which the high-efficiency plateau extends to St = 0.60 for $\alpha_{max} = 19-27°$.

For $\alpha_{max} = 25°$, higher-order heave motion experiments were conducted at $\psi = [80, 100]°$. The trends are the same as at lower α_{max}, but very high values of C_T are now possible. For $\psi = 80°$ and St = 0.60, for instance, efficiency increases slightly from 54 to 57%, and thrust coefficient improves from 0.79 to 1.73. For $\psi = 100°$, efficiency at St = 0.60 increases from 44 to 53%. The thrust coefficient here improves from 1.11 to 2.09.

The higher-order heave motion experiments are quite encouraging. Small changes in the heave motion can effect drastic changes in performance by preventing corrupted angle of attack profiles. Since the distorted angle of attack profile is no longer present, the performance decline caused by phase angles other than 90° is largely negated. The highest thrust coefficient recorded in this work occurred during one of these experiments ($C_T = 2.43$ for $\psi = 100°$, $\alpha_{max} = 30°$). These results suggest that controlling the angle of attack through slight modifications to foil motion should be studied further.

Table 2
Effects of higher-order heave motion to eliminate distortion in the angle of attack. C_T and η values for the nominal case of sinusoidal heave motion are from the contours of Figs. 6–9

α_{max}	ψ	St	C_T (nom.)	C_T (fixed)	η (nom.)	η (fixed)
15°	80°	0.32	0.30	0.32	0.61	0.56
		0.36	0.25	0.37	0.52	0.57
		0.40	0.16	0.43	0.40	0.60
	90°	0.48	0.80	0.82	0.61	0.58
		0.52	0.78	0.95	0.56	0.59
		0.56	0.72	1.06	0.50	0.56
		0.60	0.58	1.21	0.41	0.56
	100°	0.32	0.33	0.41	0.52	0.58
		0.36	0.31	0.44	0.45	0.52
		0.40	0.18	0.54	0.25	0.51
20°	80°	0.40	0.60	0.69	0.63	0.61
		0.44	0.51	0.77	0.57	0.60
		0.48	0.41	0.88	0.52	0.61
		0.52	0.18	0.90	0.40	0.57
	90°	0.48	1.21	1.11	0.60	0.59
		0.52	1.31	1.31	0.59	0.60
		0.56	1.39	1.52	0.58	0.59
		0.60	1.45	1.71	0.58	0.58
	100°	0.40	0.74	0.83	0.58	0.58
		0.44	0.72	1.01	0.52	0.59
		0.48	0.59	1.12	0.42	0.57
		0.52	0.32	1.25	0.23	0.55
25°	80°	0.52	1.04	1.38	0.58	0.57
		0.56	0.97	1.52	0.58	0.56
		0.60	0.79	1.73	0.54	0.57
	100°	0.52	1.33	1.61	0.54	0.54
		0.56	1.29	1.89	0.51	0.55
		0.60	1.11	2.09	0.44	0.53
30°	100°	0.52	1.77	1.78	0.50	0.49
		0.56	1.96	2.06	0.51	0.48
		0.60	2.15	2.43	0.52	0.49

3.4. Braking

As noted in Fig. 3, two solutions to the angle of attack equation exist. One of these solutions has an instantaneous lift vector with a component in the thrust direction, and the other solution has a component in the drag direction. One small set of runs was conducted to examine the performance of the foil in a slowing, or braking, situation. For $\alpha_{max} = 30°$, $\psi = 90°$, and $h_0/c = 1.0$, the drag-producing value of θ_0 was used and the results compared to thrust producing runs using the same parameters. Results are shown in Fig. 14.

Unlike the thrust-producing solution, which produces drag at low Strouhal number and transitions to thrust as Strouhal number increases, the drag solution produces a negative value of thrust coefficient over the entire range of Strouhal numbers tested. The magnitude of the drag force can be more than twice as large as the magnitude of the thrust force, for example at St = 0.40.

It should be noted that braking forces are likely to be transient in applications. Unlike a steady propulsion condition, the vehicle would slow down under the braking forces, leading to a change in the flow conditions and hence the braking force. In contrast, the experiments reported here were at a constant towing speed. Nonetheless, changing to a reversing

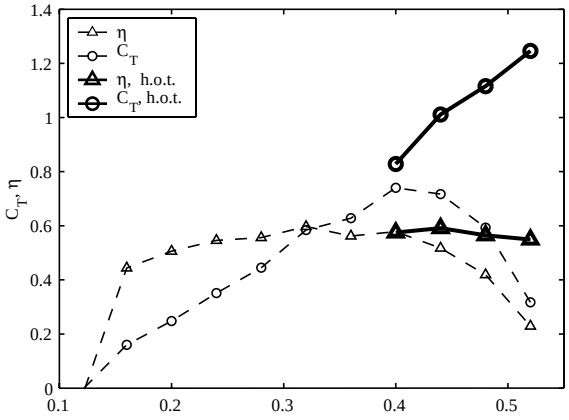

Fig. 13. Effect of higher-order heave motion for $\alpha_{max} = 20^\circ$, $\psi = 100^\circ$, $h_0/c = 1.00$. The correction leads to substantially improved lift coefficients, with nearly constant efficiency, at the higher Strouhal numbers.

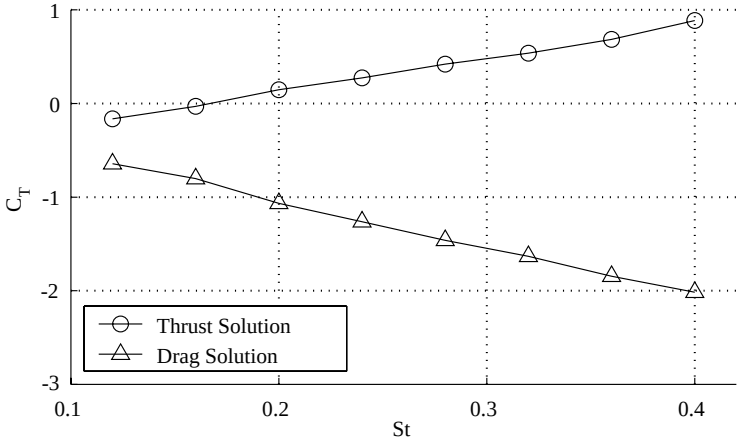

Fig. 14. Braking effect, achieved by choosing the drag solution for θ_0.

force simply by increasing θ_0 could be quite convenient in engineering use. Instead of reversing propeller pitch or using a reversing gear set, a foil-propelled vehicle could increase pitch amplitude, according to Fig. 3, to slow down.

4. Maneuvering with an oscillating foil

4.1. Pitch bias

During straight-line, symmetric propulsion, an oscillating foil device produces instantaneous force vectors with relatively small thrust components. Most of the force produced by the foil is in the form of lift; symmetry causes the mean lift to be zero. By adding a bias, or static offset, to the angle of attack, one can take advantage of these large lift forces for maneuvering. The simplest method is to add bias to the pitch angle itself, which is linearly related to the angle of attack.

Experiments were conducted in the parameter space of good thrust production in propulsion: $\psi = 90^\circ$, $\alpha_{max} = [25, 30, 35]^\circ$. A phase angle of 100° was also tested at $\alpha_{max} = [30, 35]^\circ$ since these runs produced very high thrust in straight propulsion. All pitch biases were positive to direct flow away from the free surface; the heave motion was $h_0/c = 1.00$. For each set of parameters, the mean lift and thrust coefficient over one cycle are given. Since these forces would be transient in a real application, the maximum instantaneous lift coefficient is also recorded.

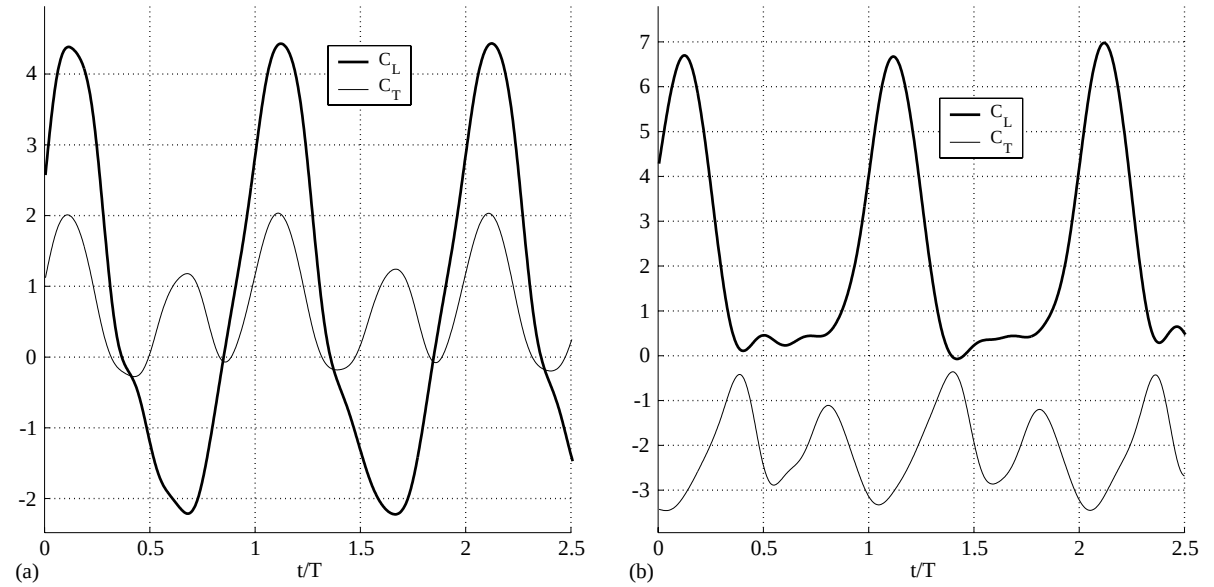

Fig. 15. Lift and thrust coefficient traces during bias tests, $\psi = 90^\circ$, $\alpha_{max} = 25^\circ$, St = 0.40: (a) bias = 10°; (b) bias = 60°. Increasing the bias angle causes a decrease in mean thrust and an increase in mean lift.

Example time traces in Fig. 15, for bias angles of 10° and 60°, verify the desired effect. With a small bias angle, the vertical force possesses an asymmetry with both positive and negative regions. The thrust force varies at twice the frequency as expected, and has short periods of negative (drag) force. Larger bias angles create vertical forces which are of one sign only, and characterized by strong peaks. The concurrent horizontal force is entirely in the drag direction.

The mean lift and thrust coefficients are given in Fig. 16, wherein the horizontal axis represents C_T and the vertical axis C_L. Each curve covers a range of bias angles; the zero bias angle always provides near zero mean lift. Adding a pitch bias always decreases the thrust coefficient, although small bias angles still produce useful amounts of thrust. Finally, the effects of high St seem to diminish in the drag regime; above 30° bias angle, the thrust coefficient appears to be almost independent of St. The data for St = 0.60 are summarized in Table 3.

We are merging our control surface and propulsor into one device, so that comparing the forces reported here to, say, the lift to drag (L/D) ratio of a wing or rudder is difficult. The magnitude of both drag and thrust achieved here is generally much larger than the steady drag of a streamlined wing, leading to low ratios of L/D relative to these wings. On the other hand, we can also produce a pure lift force. In this case the drag would approach zero and L/D would approach infinity. In any event, the values of mean lift are large relative to a steady flow case. For the case of a 30° bias, the angle of attack over one cycle will have a minimum of 0° and maximum of 60° (when non-biased maximum angle of attack is 30°). The stall angle for a NACA 0012 foil is approximately 16°, so stall is likely taking place over part of each cycle. A rudder of this equivalent section would have a steady maximum lift coefficient of about 1.6, at 16° angle of attack, just before stall. The very large values of mean lift coefficients we have observed could only be obtained in steady flow using multiple slat and flap wings or boundary layer control.

Comparing the estimated mean lift coefficients achieved at zero thrust level (Table 4), we note that 100° phase angle shows slightly more mean lift. We also note that 30° maximum angle of attack (with respect to zero bias angle) shows the highest performance in both the 90 and 100° phase angle cases. The estimated bias angles resulting in zero thrust force are quite close together near 24.5°, even though there is a 10° difference in α_{max}.

Pitch bias is a simple and effective way to obtain maneuvering forces from a foil propulsion system, through unsteady effects. Extremely large drag forces can also be generated, exceeding those of the symmetric braking solution discussed in Section 4.

4.2. Impulsive starting

A related problem in maneuvering involves forces created when the foil moves through a single sweep, in still water. A smooth trajectory is illustrated in Fig. 17, wherein the trailing edge sweeps out an arc as the heave and pitch go through half-sinusoidal trajectories, with finite acceleration. We performed tests also with other trajectories, but found

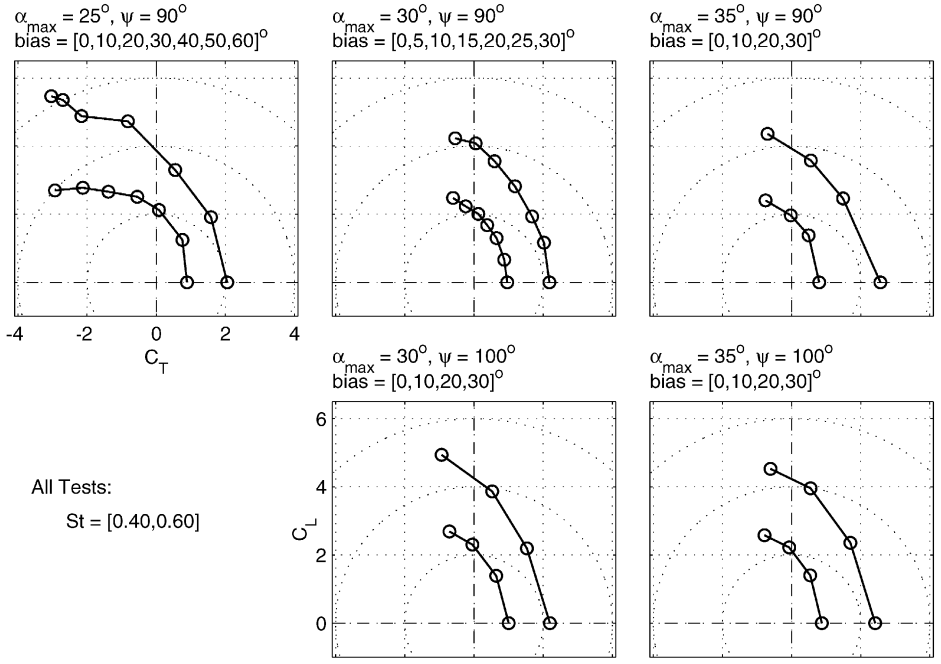

Fig. 16. Mean C_T and C_L points for tests with pitch bias.

Table 3
Force coefficients for 30° pitch bias, St = 60.

ψ	α_{max}	C_T	C_L	$C_L(max)$
90°	25°	−0.82	4.7	11.9
90°[a]	25°	−3.04	5.5	16.6
90°	30°	−0.55	4.2	12.7
90°	35°	−0.70	4.4	13.5
100°	30°	−0.94	4.9	13.3
100°	35°	−0.61	4.5	13.8

[a] bias angle 60°.

Table 4
Estimated pure lift coefficients and bias angles for zero thrust, St = 0.60

ψ	α_{max}	C_L	Bias
90°	25°	3.94	24.3°
90°	30°	4.07	25.4°
90°	35°	3.93	24.5°
100°	30°	4.34	24.0°
100°	35°	4.29	24.1°

ringing in the force signals whenever the velocity was discontinuous. The force response (Fig. 18) is typified by a single large peak in lift force, and two smaller peaks in thrust, which are obviated by a long drag period following. In the data shown, the drag period occurs after the motion is complete.

Nondimensionalization of the forces is performed using the usual lift and drag coefficients, but with the maximum heave velocity. Instantaneous thrust and lift values scale closely with this reference velocity squared, causing the coefficients to take roughly constant values; see Table 5. Since the motions are harmonic, the forces can be correlated

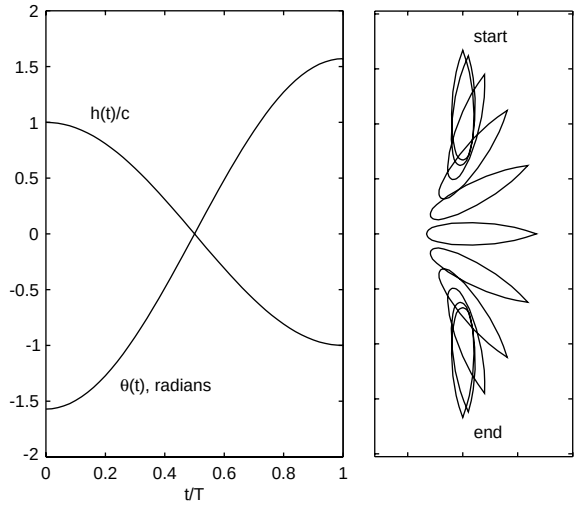

Fig. 17. Foil trajectory for an impulsive starting maneuver, comprising a single downward heave stroke, with a 180° pitch change.

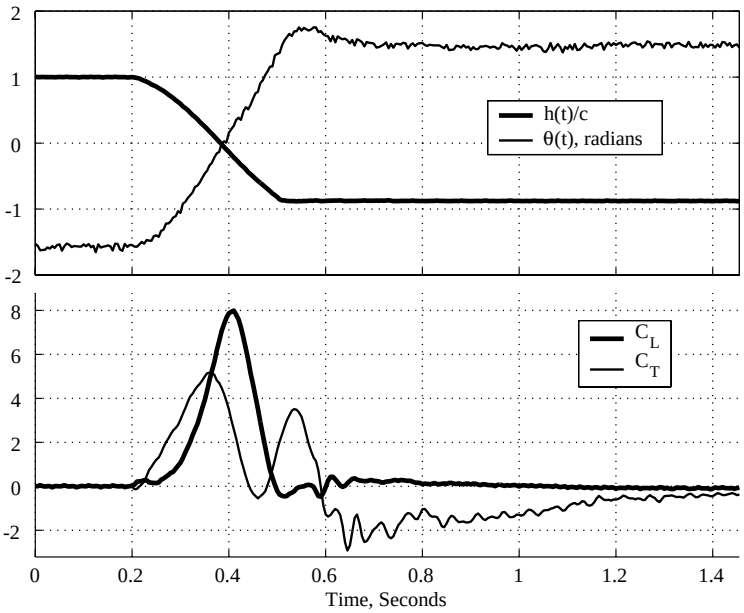

Fig. 18. Results of an impulsive starting maneuver, with maximum heave velocity 0.754 m/s. Top: heave and pitch motion, bottom: lift and thrust coefficients. Lift is characterized by a single peak, whereas thrust has two peaks, and then a long period of moderate drag.

Table 5
Instantaneous thrust and lift coefficients during a one-time starting maneuver, showing the sizable, transient lateral forces that accompany mean thrust production

$\dot{h}(max)$	$C_T(max)$	$C_L(max)$
0.50	5.4	7.9
0.57	5.5	8.3
0.63	5.1	7.7
0.69	5.3	8.1
0.75	5.3	8.0

directly with acceleration, and hence with added mass. Consequently, no upper limit exists for the fluid forces which can be generated; rather, the constraint is the force which can be sustained by the device.

5. Discussion and summary

5.1. Propulsion

Under proper conditions, the propulsive performance of an oscillating foil is good. The highest propulsive efficiency we achieved was 71.5% at the settings $\alpha_{\max} = 15^\circ$, $\psi = 90^\circ$, and $\mathrm{St} = 0.16$. The corresponding thrust coefficient was 0.18, in line with the generally good efficiency of lightly loaded propulsors. Two very high thrust coefficients were achieved. A value of $C_T = 2.41$ ($C_{T_{SA}} = 1.205$) occurred at $\alpha_{\max} = 35^\circ$, $\psi = 100^\circ$, and $\mathrm{St} = 0.60$; corresponding efficiency was $\eta = 43.2\%$. A thrust coefficient of 2.43 ($C_{T_{SA}} = 1.215$) occurred during one experiment with higher-order heave motions, with $\alpha_{\max} = 30^\circ$, $\psi = 100^\circ$, and $\mathrm{St} = 0.60$; the efficiency was 49%. Besides these maxima, we can also note efficiency plateaus in both the $h_0/c = 0.75$ and 1.00 cases. These plateaus represent large areas of the parameter space in which routine efficiencies greater than 50% can be achieved. Finally, there are conditions for which higher C_T could be expected, if St can be increased beyond the limits of our experiment. In particular, the higher-order heave correction may extend the high-efficiency plateau significantly.

The performance gains induced by the high-order heave corrections are made by altering the heave motion only slightly; the expansion of $atan(x)$ requires heave corrections of about 6% for $\mathrm{St} = 0.60$. On the other hand, since small changes in heave motion result in large changes in performance, we can conclude that the problem is sensitive to heave; further investigations which allow pitch angle to vary also would be illuminating.

The parametric study described in Fig. 3 can be tied to the propulsion results, by noting that the parameter space we investigated involves α profiles of several forms. The form of the profile is either sinusoidal, flattened, or multi-peaked; the multi-peaked profiles have either four or six peaks per cycle. Several transition lines are shown in Fig. 19, and Fig. 4 is a reference. Line 1 is the condition at which $\theta_0 = 0$, i.e., there is no pitch motion. Line 2 is the condition for a perfectly flattened sinusoid, *before* multiple peaks begin to appear. Line 3 is the condition at which the angle of attack reaches zero four times per cycle. Finally, Line 4 represents the terminal Strouhal number, beyond which solutions are unavailable. All points in the parameter space to the left of line 2 have a generally sinusoidal α profile, becoming closer to a square wave as they approach line 2. Points between lines 2 and 3 have four peaks per cycle, but no more than two zero crossings. Points *on* line 3 have four peaks per cycle and four zero values. Points between lines 3 and 4 have six peaks per cycle and six zero crossings. Four of these peaks are at the maximum angle of attack and two are smaller. Points *on* line 4 actually reach the maximum angle of attack six times per cycle.

Some of these calculated contours can be useful for predicting propulsion results. For instance, the line describing $\theta_0 = 0$ estimates the low-St zero thrust contour fairly well. Similarly, the small range of high-St zero-thrust contour measured here is predicted quite well by line 3, where the first reversal of α occurs. These two lines form a good estimate of the thrust-producing region of the parameter space. Perhaps more useful, line 2 closely predicts the angle of attack for maximum thrust coefficient for Strouhal numbers above 0.40; at lower St, it specifies more efficient solutions.

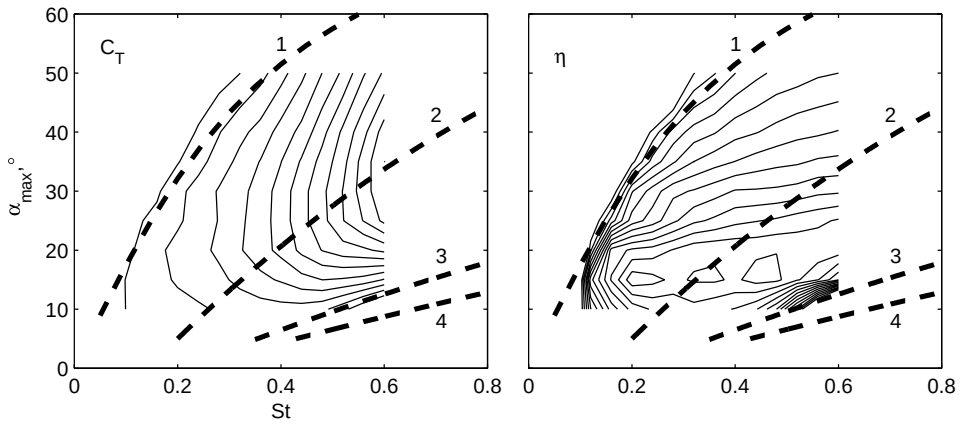

Fig. 19. Thrust coefficient and efficiency contours with overlays of: $\theta_0 = 0$ (1), a flattened α-profile, with no extra peaks (2), α reaching zero four times per cycle (3), the terminal Strouhal number (4).

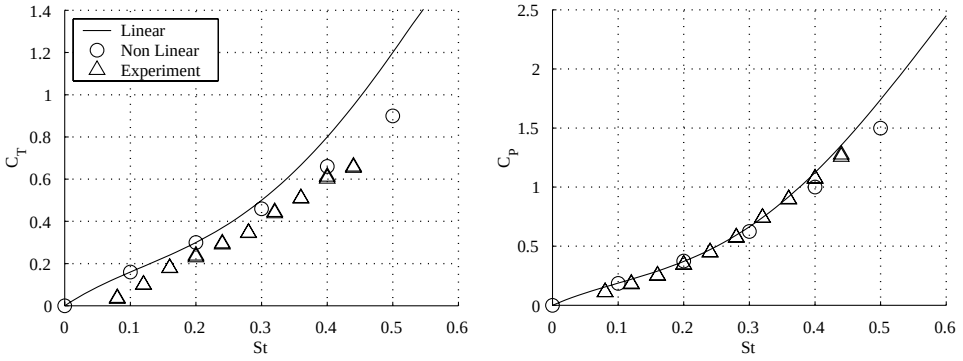

Fig. 20. Thrust coefficient C_T and power coefficient C_P compared to theoretical/numerical results (Anderson et al., 1998). The consistent discrepancy in thrust coefficient is due to drag on the foil, which is not accounted for in the theoretical and numerical results shown.

In contrast to thrust coefficient, the band of high efficiency occurs over three angle of attack profile regions: sinusoidal, flattened, and quadruple peaked. This behavior may be due to the fact that while thrust performance correlates directly with the angle of attack profile, the efficiency is more closely related to the *wake* structure, which cannot be so easily predicted from the angle of attack.

The data from these experiments can also be compared with results from linear and nonlinear analytical and numerical methods, as described by Anderson et al. (1998). In Fig. 20, the thrust coefficients from our experiment are consistently less than the theoretical values. As mentioned previously, however, our thrust values are measured using $U = 0$ as the zero level for thrust. Employing the nominal foil drag as the zero would therefore result in a higher thrust coefficient; a portion of the offset between experiment and theory is clearly due to the exclusion of foil friction drag in the theory. Looking at the power coefficient, we see that the experimental and theoretical data match quite well in the range tested. The resulting efficiency points (not shown) reveal trends similar to the thrust coefficient, with a consistent offset above $\mathrm{St} = 0.15$.

As a specific comparison with previous experiments, under the conditions of $h_0/c = 0.75, \alpha_{\max} = 15^\circ, \psi = 90^\circ, \mathrm{St} = 0.22$, Anderson et al., in their Fig. 8, obtain 78% efficiency. Making an allowance for drag involves a thrust reduction of $\delta C_T \simeq -0.05$; this value can be obtained from the literature, e.g., Hoerner (1965), or by experiment (Haugsdal, 2001). The true efficiency, including drag, then is reduced to 0.67. This point is in excellent agreement with Figs. 6 and 7 herein. On the other hand, the extraordinary efficiencies reported in Anderson et al.'s Fig. 9 ($h_0/c = 0.75, \alpha_{\max} = 15^\circ, \psi = 75^\circ, \mathrm{St} = 0.18, C_T = 0.28, C_P = 0.32, \eta = 0.87$ (0.72 corrected for drag)) are not supported by our experimental results. We found almost uniformly that $\psi = 90^\circ$ provides the best thrust and efficiency, and that what little improvement is available is made by increasing ψ, not reducing it. Under the specific conditions noted above, we found $C_T = 0.16, C_P = 0.26, \eta = 0.61$. While this discrepancy between experiments remains unresolved, it should be pointed out that the low values of C_T and particularly of C_P make the efficiency calculation quite susceptible to measurement error.

5.2. Maneuvering

Maneuvering tests with the oscillating foil are very promising. By adding pitch bias to the harmonic motion, large lift coefficients can be achieved; the largest mean and instantaneous values are $C_L = 5.5$ and 16.6, respectively. These values were achieved for Strouhal number 0.60, the maximum level we could achieve with our apparatus. Therefore it seems likely that even larger values would be possible for higher St. Large lift values are generally accompanied by a large drag force, representing a braking force in the context of a marine vehicle. For certain values of $\alpha_{\max}$ near 25°, referenced to zero-bias case, zero drag can be achieved. The highest pure mean lift coefficient was 4.3 at $\psi = 100^\circ$ and $\alpha_{\max} = 30^\circ$; the estimated bias angle was 24.0°. The bias angle for pure lift was fairly consistent for the parameters tested, varying between 24 and 25.4°, even though $\alpha_{\max}$ varied by 10° in the experiments. In fact, the total force vectors for pitch bias cases are always larger than those of propulsion cases, as illustrated by comparing Figs. 15 and 10.

The lift coefficient due to a bias increases with Strouhal number, the highest values always occurring at the highest tested Strouhal number of 0.60, or a reduced frequency of $k = 0.94$. In comparison, the oscillating flow experiments of

Gursul and Ho (1992) indicated an optimum value of about $k = 0.80$, where their lift coefficients showed a maxima. Another estimate for the optimum k, based on vortex wavelength, is $k \approx 1$. Hence, it is possible that our Strouhal number limit is near an optimum value, and that the lift coefficient would begin to decrease if higher Strouhal numbers could be tested.

Impulse starts of the foil revealed that very large starting forces can be created, apparently limited only by the speed and structural strength of the apparatus. Tests were performed in which the foil performed one half-cycle of heave motion on a stationary carriage, while undergoing 180° of pitch. The time signal indicates an extremely large lift force is possible, with instantaneous C_L of about 8.0. The lift is accompanied by two smaller positive peaks in thrust, and a long period of drag which yields essentially no net propulsion.

5.3. Concluding remarks

Propulsive and maneuvering tests on an oscillating NACA 0012 foil provide systematic data on the thrust and side force production in harmonically flapping foils. Propulsive tests show good thrust production for certain parametric combinations of the heave amplitude, Strouhal number, angle of attack and phase angle between heave and pitch. For high Strouhal numbers, the thrust coefficient deteriorates rapidly because the induced angle of attack ceases to be a harmonic function of time. A properly selected introduction of higher harmonics in the heave motion, so as to reduce the angle of attack to a pure harmonic, increases substantially the thrust coefficient. Systematic introduction of transient motion, either in the form of a bias angle, or suddenly starting harmonic motion, produces substantial transverse forces, capable of inducing maneuvering motions to a vehicle equipped with flapping foils. Mean lift coefficients of up to 5.5 and instantaneous coefficients of up to 16 were measured. Higher values seem possible for higher Strouhal numbers. As a result, flapping foils are found to be outstanding devices for producing transient forces for maneuvering and control of marine vehicles.

Acknowledgements

Support by the Office of Naval Research, under contract number N00014-99-1-1082 and monitored by Dr Teresa McMullen, and the MIT Sea Grant Office under contract number NA86RG0074, is gratefully acknowledged. D.R. was also supported by the MTS Systems Corporation George Butzow Fellowship.

References

Anderson, J.M. 1996. Vorticity control for efficient propulsion. Ph.D. Dissertation, Department of Ocean Engineering, Massachusetts Institute of Technology, Cambridge, MA, USA.

Anderson, J.M., Streitlien, K., Barrett, D.S., Triantafyllou, M.S., 1998. Flapping foils of high propulsive efficiency. Journal of Fluid Mechanics 360, 41–72.

Bandyopadhyay, P., Castano, J., Rice, J., Phillips, R., Nedderman, W., Macy, W., 1997. Low-speed maneuvering hydrodynamics of fish and small underwater vehicles. Journal of Fluids Engineering 119, 136–144.

Cheng, H.K., Murillo, L.E., 1984. Lunate-tail swimming propulsion as a problem of curved lifting line in unsteady flow. Part 1: symptotic theory. Journal of Fluid Mechanics 143, 327–350.

Cortelezzi, L., Chen, Y.-C., Chang, H.-L., 1997. Nonlinear feedback control of the wake past a plate: from a low-order model to a higher-order model. Physics of Fluids 9, 2009–2022.

Dickinson, M.H., Lehmann, F.-O., Sane, S., 1999. Wing rotation and the aerodynamic basis of insect flight. Science 284, 1954–1960.

Drucker, E.G., Lauder, G.V., 1999. Locomotor forces on a swimming fish: three-dimensional wake dynamics quantified using digital particle image velocimetry. Journal of Experimental Biology 202, 2393–2412.

Ellington, C.P., 1984. The aerodynamics of hovering insect flight. V: A vortex theory. Philosophical Transactions of the Royal Society of London B 305, 115–144.

Ellington, C.P., Van den berg, C., Thomas, A., 1996. Leading edge vortices in insect flight. Nature 384, 6–26.

Freymuth, P., 1988. Propulsive vortical signature of plunging and pitching airfoils. AIAA Journal 26, 881–883.

Freymuth, P., 1990. Thrust generation by an airfoil in hover modes. Experiments in Fluids 9, 17–24.

Gopalkrishnan, R., Triantafyllou, M.S., Triantafyllou, G.S., Barrett, D.S., 1994. Active vorticity control in a shear flow using a flapping foil. Journal of Fluid Mechanics 274, 1–21.

Gursul, I., Ho, C.M., 1992. High aerodynamic loads on an airfoil submerged in an unsteady stream. AIAA Journal 30, 1117–1119.

Hart, D., Acosta, A., Leonard, A., 1992. Observations of cavitation and wake structure of unsteady tip vortex flows. In Proceedings of the International STG Symposium on Propulsors Cavitation Hamburg, Germany, pp. 121–127.

Haugsdal, O., 2001. Motion control of oscillating foils for steady propulsion and starting maneuvers. Sivilingenior Thesis, NTNU Department of Marine Technology.

Hoerner, S.G., 1965. Fluid-dynamic Drag. Hoerner Fluid Dynamics, Bakersfield, CA.

Hoppe, K.G., 1989. The dynamo-elastic oscillating foil propeller. Schiff Hafen 5, 54–61.

Kato, N., 1998. Locomotion by mechanical pectoral fins. Journal of Marine Science and Technology 3, 113–121.

Koochesfahani, M.M., Dimotakis, P., 1988. A cancellation experiment in a forced turbulent shear layer. AIAA Technical Paper 88-3713-CP.

Koochesfahani, M.M., 1989. Vortical patterns in the wake of an oscillating airfoil. AIAA Journal 27, 1200–1205.

Liu, H., Ellington, C.P., Kawachi, K., Van den berg, C., Wilmlmott, A.P., 1998. A computational fluid dynamic study of hawkmoth hovering. Journal of Experimental Biology 201, 461–477.

Lighthill, M.J., 1969. Hydromechanics of aquatic animal propulsion. Annual Review of Fluid Mechanics 1, 413–445.

Luznik, L., Bose, N., 1998. Propulsive thrust of an oscillating foil at large angles of attack: experimental study. Proceedings of the American Towing Tank Conference Iowa City, IA, pp. 1–8.

Maresca, C., Favier, D., Rebont, J., 1979. Experiments on an airfoil at high angle of incidence in longitudinal oscillations. Journal of Fluid Mechanics 92, 671–690.

Maxworthy, T., 1979. Experiments on the Weis-Fogh mechanism of lift generation by insects in hovering flight. Part I: dynamics of the fling. Journal of Fluid Mechanics 93, 47–63.

McCroskey, W.J., 1982. Unsteady airfoils. Annual Review of Fluid Mechanics 14, 285–311.

Ohmi, K., Coutanceau, M., Loc, T.P., Dulieu, A., 1990. Vortex formation around an oscillating and translating airfoil at large incidences. Journal of Fluid Mechanics 211, 37–60.

Ohmi, K., Coutanceau, M., Daube, O., Loc, T.P., 1991. Further experiments on vortex formation around an oscillating and translating airfoil at large incidences. Journal of Fluid Mechanics 225, 607–630.

Oshima, Y., Natsume, A., 1980. Flow field around an oscillating foil. In: Merzkirch, W. (Ed.), Flow Visualization II. Hemisphere, New York, pp. 295–299.

Oshima, Y., Oshima, K., 1980. Vortical flow behind and oscillating foil. In: Proceedings of the 15th International Congress; International Union of Theoretical and Applied Mechanics, Toronto, North-Holland, Amsterdam; pp. 357–68.

Rayner, J.M.V., 1979. A vortex theory of animal flight mechanics. Journal of Fluid Mechanics 91, 731–763.

Rayner, J.M.V., 1995. Dynamics of the vortex wakes of flying and swimming vertebrates. In: Ellington, C.P, Pedley, T.J. (Eds.), Biological Fluid Dynamics. Society of Experimental Biology, Cambridge, UK, pp. 131–155.

Reynolds, W.C., Carr, L.W., 1985. Review of unsteady, driven, separated flows. AIAA Paper 85-0527.

Scherer, J.O., 1968. Experimental and theoretical investigation of large amplitude oscillating foil propulsion systems. US Army Engineering Research and Development Laboratory Technical Report 662-1.

Streitlien, K., Triantafyllou, G.S., Triantafyllou, M.S., 1996. Efficient foil propulsion through vortex control. AIAA Journal 34, 2315–2319.

Triantafyllou, G.S., Triantafyllou, M.S., Grosenbaugh, M.A., 1993. Optimal thrust development in oscillating foils with application to fish propulsion. Journal of Fluids and Structures 7, 205–224.